Computations of Droplet Impingement on Airfoils in Two-Phase Flow

Sang Dug Kim*, Dong Joo Song
School of Mechanical Engineering, Yeungnam University,
214-1, Dae-dong, Gyeongsan-si, Gyeongsangbuk-do 712-749, Korea

The aerodynamic effects of leading-edge accretion can raise important safety concerns since the formulation of ice causes severe degradation in aerodynamic performance as compared with the clean airfoil. The objective of this study is to develop a numerical simulation strategy for predicting the particle trajectory around an MS-0317 airfoil in the test section of the NASA Glenn Icing Research Tunnel and to investigate the impingement characteristics of droplets on the airfoil surface. In particular, predictions of the mean velocity and turbulence diffusion using turbulent flow solver and Continuous Random Walk method were desired throughout this flow domain in order to investigate droplet dispersion. The collection efficiency distributions over the airfoil surface in simulations with different numbers of droplets, various integration time-steps and particle sizes were compared with experimental data. The large droplet impingement data indicated the trends in impingement characteristics with respect to particle size; the maximum collection efficiency located at the upper surface near the leading edge, and the maximum value and total collection efficiency were increased as the particle size was increased. The extent of the area impinged on by particles also increased with the increment of the particle size, which is similar as compared with experimental data.

Key Words: Two-Phase Flow, Particle Trajectory Simulation, Leading-Edge Accretion, Continuous Random Walk Model

1. Introduction

Aircraft flying at subsonic speeds through clouds can be subject to ice formation around the leading edge of the wing. This aerodynamic effect of leading-edge accretion can lead to deterioration of aerodynamic performance, handling qualities and important safety concerns. The understanding and certification on the aircraft icing requires massive evaluation of the extent and intensity of liquid-particle impingement. The impingement characteristics of an aircraft can be used in predicting the ice accretion around its critical aerodynamic portion and determining size and location of the ice protection system. One of the most important ways to determine the impingement characteristics and potential ice accretions on critical aerodynamic shapes is the computational fluid dynamics (CFD) which can play a significant role. It is important, however, that the methodology of CFD be validated with various experimental data. The NASA Glenn LEWICE code which adopts the potential flow solver can provide cost-effective information for predicting ice accretions on the critical aerodynamic surfaces and for design and certification of ice protection systems. Current study provides a new code to simulate particle trajectory around an airfoil and to investigate the impingement characteristics on airfoil surfaces in turbulent external flow.

* Corresponding Author,
E-mail : sangkim@yu.ac.kr
TEL : +82-53-810-3529; **FAX** : +82-53-810-4627
School of Mechanical Engineering, Yeungnam University, 214-1, Dae-dong, Gyeongsan-si, Gyeongsangbuk-do 712-749, Korea. (Manuscript **Received** June 17, 2005; **Revised** October 26, 2005)

Ground-based simulation of icing conditions is conventionally accomplished in wind tunnels with droplets injected upstream of the test section ; this is achieved through the use of nozzles where the water droplets are entrained in the wake of spay-bars in which nozzles are installed, transported downstream by the tunnel air, and then reach a super-cooled state from the sub-freezing air temperatures, and result in a dispersed cloud at the test section. A primary design consideration of the icing cloud is that the test section LWC (Liquid Water Content) should have high spatial uniformity to mimic realistic atmospheric icing characteristics around an airfoil. Thus, computational methods, which track the turbulent dispersion of the water droplets as they proceed from the nozzles to the test section, could be beneficial in understanding realistic particle trajectory and impingement characteristics on critical aerodynamic surfaces.

Most previous droplet trajectory methodologies used for icing research wind tunnels installed with an airfoil have primarily considered the mean velocity distributions with the wind tunnel (Bragg and Khoudadoust, 1995) and turbulent levels which yields the turbulent dispersion and spatial uniformity of the icing cloud (Hancir and Loth, 1999 ; DeAngelis et al., 1997). The procedure was based on a Lagrangian transport methodology for the droplet phase and consideration for spatial deviations of turbulence level, especially around airfoil surfaces, which implies that it is necessary to model the effect of turbulent diffusion. It can be seen that when the turbulence is taken into account, the particles are dispersed according to the intensity of the turbulence which results in various intensities of the droplet impingement. Thus, it is important to get an accurate prediction of the turbulence for an accurate prediction of droplet trajectories. However, the lack of quantitative fidelity was attributed to the lack of well-characterized two-phase flow around a thin shape such as an airfoil, and to the absence of a detailed simulation in experiment or in computation. As such, the objective of the present investigation is to establish a robust and accurate methodology for predicting the airflow, in particular including the turbulence diffusion around an airfoil, and to investigate the characteristics of droplet impingement as well as particle trajectory for a variety of droplet conditions.

2. Numerical Methods

A computational strategy for the simulation of the flow field in an icing wind tunnel is employed herein that, because droplet effects on gas-phase momentum are negligible due to low overall droplet mass loading (generally less than 0.5%), the gas-phase solution can be computed a priori with a single-phase flow solver. Droplet collisions are also ignored based on the highly dilute conditions of typical icing tunnels. Therefore, the methodology involves a two-part scheme : an Eulerian airflow calculation followed by Lagrangian droplet trajectory calculations. This sequential achievement enables the more efficient use of computer time when parametric studies of different particle conditions are to be completed for the same tunnel air flow conditions. In the following, the air flow and droplet trajectory methodologies are described as well as stochastic turbulent method.

2.1 Continuous-phase modeling

One of the turbulent flow techniques which can be used is the time-averaged flow descriptions, which are usually called by the unresolved-eddy simulations. This includes RANS (Reynolds-averaged Navier-Stokes) simulations which involves the solutions of the mean quantities, e.g. u_f, k and ω. The computations herein solve for the steady-state compressible turbulent flow using a finite-volume method, which includes the usage of the SST (Shear-Stress Transport) k-ω turbulence model (Menter, 1994 ; Kim and Song, 2005). This model was used since it is known to reasonably predict turbulence for free-shear flows and turbulent boundary layers with the adverse pressure gradient.

Inflow conditions for the present simulations consisted of a uniform distribution of inflow velocity, and turbulent kinetic energy (k), with a uniform distribution of the temperature, pressure,

and specific dissipation (ω). For the outflow conditions all properties were extrapolated. The wind tunnel walls were assumed to be inviscid, such that the normal components of velocity were defined to be zero.

The steady-state solution is executed iteratively on the computational grid using local time-stepping where the flow equations are evaluated using second-order-accurate finite-volume techniques. The partial differential equations are modeled in their conservative form where the explicit terms are computed using a Roe upwind second-order operator with TVD scheme (Kim and Song, 2005).

2.2 Droplet trajectory methodology

Two-way coupling in two-phase flow indicates that interphase transfer of mass, momentum or energy is important to the fluid dynamic description. Usually, the mass loading is the primary non-dimensional parameter of influence, which is defined as the particle mass per unit volume of mixture divided by the continuous-fluid mass per unit volume of mixture, ρ_p/ρ_f. Mass loading affects changes in the momentum of the fluid. Thus one can expect the fluid variations to be unaffected by the particles if the mass loading is small. For the NASA Glenn IRT (Icing Research Tunnel), the mass loading is typically 10^{-3}. Based on the above-described criteria the level of coupling for the IRT reduces from a two-way to a one-way coupling. By these assumptions, particle-laden two-phase flows can be characterized by a single-phase gas flow field carrying particles, which react solely to aerodynamic drag from the gas. Reaction of the particles to the gas turbulence in terms of their trajectories is called turbulent dispersion, and is discussed in the following section.

Kuo gives the general equation of particle motion for a spherical particle (Kuo, 1986) as:

$$\frac{\pi}{6}d_p^3\rho_p\frac{d\vec{U}_p}{dt}=\frac{\pi}{8}d_p^2C_D\rho_f|\vec{U}_f-\vec{U}_p|(\vec{U}_f-\vec{U}_p)+\vec{F}_2+\vec{F}_3+\vec{F}_4+\vec{F}_e \quad (1)$$

where $\vec{U}_f$ and $\vec{U}_p$ are the gas and particle velocities, ρ_f and ρ_p are the gas and particle densities, d_p is the particle diameter, C_D is the drag coefficient for a sphere (a function of particle Reynolds number) and $\mathbf{F}_e$ is external or body force. The terms $\mathbf{F}_2$, $\mathbf{F}_3$ and $\mathbf{F}_4$ account for forces dealing with static pressure gradients, virtual mass and Basset force. In dilute systems such as current wind tunnel flow, however, particle-particle collisions can also be ignored, thus the relevant particle equation of motion can be written as

$$\frac{\pi}{6}d_p\frac{d\vec{U}}{dt}=\frac{\pi}{8}d_p^2C_D\rho_f|\vec{U}_f-\vec{U}_p|(\vec{U}_f-\vec{U}_p)+\frac{\pi}{6}d_p^3\rho_pg \quad (2)$$

Coupled with the Navier-Stokes equations for a single-phase gas, Eq. (2) can be solved for the particle velocity. Unfortunately, the Navier-Stokes equations for turbulent flows can only be approximated in a statistical sense for most complex flows given current computational constraints.

In the following, we describe the particle phase governing equations followed by the stochastic model for simulating turbulent velocity fluctuations to allow incorporation of turbulent diffusion. Particle movement is dictated by the equations of motion for position and velocity. The particle position can be solved by the following equation:

$$\frac{d\vec{x}_p}{dt}=\vec{U}_p \quad (3)$$

where $\vec{x}_p$ is the particle location and $\vec{U}_p$ is the particle velocity. The particle acceleration is only affected by aerodynamic drag and gravity if the particle density is much greater than the gas density. Thus, the particle velocity can be found by solving an equation of motion for a spherical droplet of radius r_p.

$$\frac{d\vec{U}_p}{dt}=\frac{3}{8}\frac{\rho_f}{\rho_p}\frac{|\vec{u}_f+\vec{u}_f'-\vec{U}_p|}{r_p}(\vec{u}_f+\vec{u}_f'-\vec{U}_p)\times C_D+g \quad (4)$$

In this equation, u_f' is the instantaneous fluctuating component of the gas velocity, g is the acceleration due to gravity, and C_D is the droplet drag coefficient. Because all particles are con-

sidered spherical, C_D is taken to be:

$$C_D=\begin{cases}\dfrac{24}{\mathrm{Re}_p}\left(1+\dfrac{\mathrm{Re}_p^{2/3}}{6}\right) & \text{if } \mathrm{Re}_p<1000\\ 0.424 & \text{otherwise}\end{cases} \quad (5)$$

where

$$\mathrm{Re}_p=\frac{\rho_f|\vec{u}_f+\vec{u}'_f-\vec{U}_p|d_p}{\mu_f(\hat{T})} \quad (6)$$

The particle dynamic equation is computed using a semi-implicit time marching scheme described by Bocksell and Loth (Bocksell and Loth, 1998) where temporal resolution is assured to be sufficient. The method for determining $\vec{u}'_f$ needed in Eq. (4) is discussed in the following section.

2.3 Stochastic eddy Model

Droplets are advected based on the combination of mean velocity and a stochastic turbulent velocity fluctuation for the gas flow. For the CRW (Continuous Random Walk) method, the integral length and time scales from the SST k-ω turbulence description of the gas-phase, along with a random number generator, are used to simulate the chaotic instantaneous fluid velocity fluctuation as seen locally by the particle ($\vec{u}'_f$).

This fluctuation is combined with the local mean velocity vector to compute the trajectory of particles in the flow and to obtain mean particle diffusion characteristics. A discrete Markov chain is used to correlate the continuous-phase velocity fluctuation with the value at the previous time step along the particle path as follows:

$$\vec{u}'_f(t+\Delta t)=\Psi_p\vec{u}'_f(t)+(1-\Psi_p^2)^{1/2}\gamma(t)\left(\frac{2}{3}k\right)^{1/2}+\delta\vec{u}'_f \quad (7)$$

where $\Psi_p=\exp(-\Delta t/\tau_{\mathrm{int}})$ and γ is a random number vector selected from a Gaussian distribution and sampled every time-step and for each Cartesian direction. It is noted that the time-step size constraint allowed for statistical independence of mean particle diffusion. The interaction time scale (τ_{int}) is given by the minimum of an eddy lifetime (t_e) and a particle-eddy transit time (t_t):

$$\tau_{\mathrm{int}}=\min(t_e,\ t_t) \quad (8)$$

$$t_t=(\Lambda/U_{rel}) \quad (9)$$

where Λ represents the eddy size in all three directions. This interaction timescale can capture both the effects of eddy crossing and eddy lifetime as defined by Snyder and Lumley (1971).

Applications of the above CRW technique for non-homogeneous shear flows (wakes and jets) for short and long integration times (compared to t_A) shows that it provides high fidelity for mean particle diffusion. An example of the reasonable prediction for transverse particle diffusion in the grid-generated wake data of Snyder and Lumley (1971) is shown in Fig. 1.

Non-homogeneous turbulence causes a change in the mean pressure gradient. This is accounted for in the following drift correction term, which is essentially the isotropic analog of the drift suggested for the CRW by MacInnes and Braco (1992). The CRW formulation employs the non-empirical drift correction for non-homogeneous flows based on application of continuity to the mean Lagrangian derivative. For isotropic turbulence with no cross-correlations used to create the stochastic $\vec{u}'_f$ this is given as:

$$\delta\vec{u}'_f=-\Delta t\frac{2}{3}\frac{\partial k}{\partial\vec{x}} \quad (10)$$

This drift correction was validated over long integration times in a simple 1-D flow with a uniform mean velocity and a turbulence intensity which only varies transversely (Yuu et al., 1978).

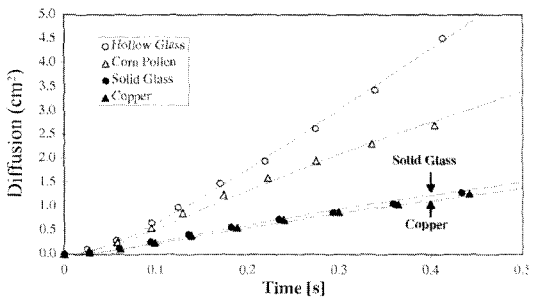

Fig. 1 Comparison of mean particle diffusion experimental data of Snyder and Lumley (1971) in grid-generated turbulence with the numerical simulations using CRW model

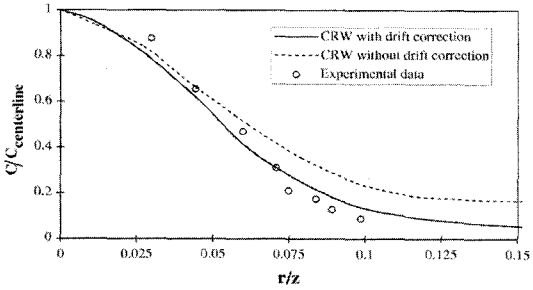

Fig. 2 Comparison of mean particle diffusion experimental data of Yuu et al.(1978) in a turbulent round jet with the numerical simulations using CRW model with and without drift correction

Figure 2 shows particle concentration normalized by centerline value as a function of radial position normalized by axial position.

3. Results

The geometry of the MS-0317 airfoil is shown in Fig. 3. In this instance, a wing spanning the entire test section domain with an MS-0317 airfoil at zero degree angle of attack is to be simulated within the test section of the NASA Glenn IRT. The commercial grid generation package GRIDGEN was used to create the 2D computational domain using the airfoil coordinates for the MS-0317 scaled accordingly. The particle trajectory code is designed to accept general grid types. Next, a 305×100 point O-type grid was generated in GRIDGEN, thus, the index of the ξ-direction begins at the trailing edge of this airfoil, and advances along the lower surface and ends back at the trailing edge. The first index of the η-direction corresponds to the surface of the airfoil.

The air flow to be used with a particle trajectory code is the result of a simulation of the test section portion of the NASA Glenn IRT with an airfoil present. Figure 4 depicts the velocity vectors near the leading edge of an MS-0317 airfoil where most particles can impinge on. As shown in Fig. 4, the surface area where the ice formation can occur due to the impingement of droplets is the critical portion to the aerodynamic performance of an airfoil. The MS-0317 airfoil is representative of modern medium speed airfoils. It was designed in the mid 1970's for general aviation aircraft. The maximum thickness for this airfoil is 0.17% of t_{max}/c at 37.5% chord, which models used in experimental and numerical simulations have a nominal code of 0.914 meters. The surface pressure coefficients of the simulated results were compared with the experimental data obtained by Papadakis et al.(2003) in Fig. 5. This figure shows the agreement of pressure coefficients between the current result of numerical simulation and the experimental data except the latter half

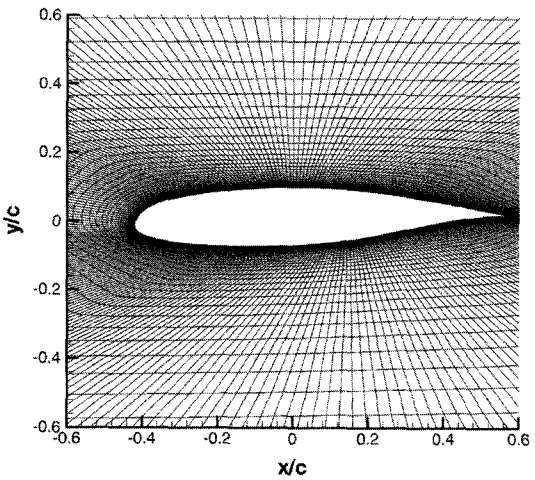

Fig. 3 Grid system around an MS-0317 airfoil

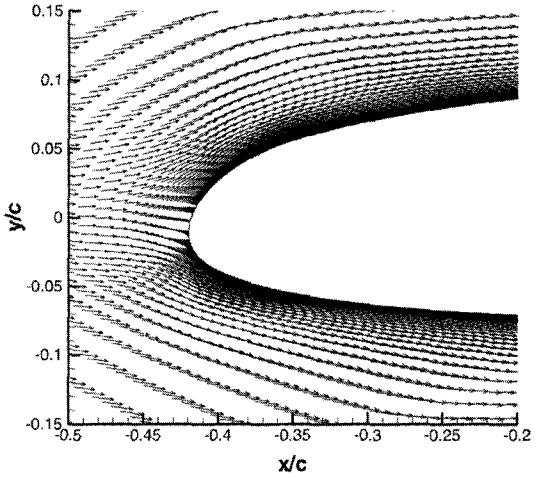

Fig. 4 Velocity vectors around the leading-edge of an MS-0317 airfoil

of the bottom surface formed by the concave where no particle can hit.

A particle trajectory code was ultimately used in combination with the validated airflow solution to calculate the collection efficiency (β) as follows:

$$\beta=\frac{\text{mass impinging on the unit area of airfoil surface}}{\text{mass per unit area on inlet boundary}} \quad (11)$$

The very big particle can be expected to move in the direction of inertia around the airfoil as it was injected on the inlet boundary. The collection efficiency of ideal case can be expressed by the function of the surface angle as shown in Fig. 6. The collection efficiency distribution for a median volumetric diameter (MVD) of 1000 μm was compared with the theoretical limit which is the absolute value of sine of the surface angle.

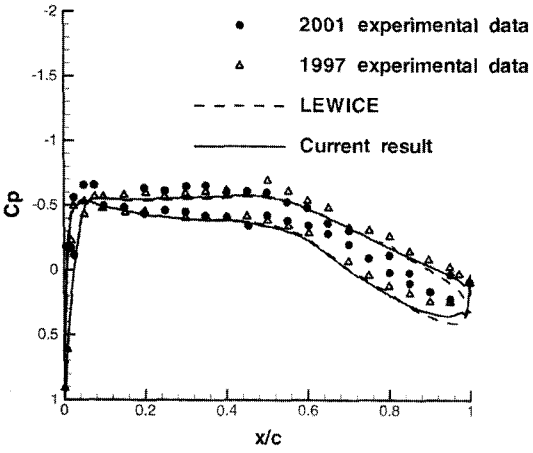

Fig. 5 Comparison of surface pressure coefficient distributions among the experimental data of Papadakis et al. (2003), LEWICE and current numerical results for an MS-0317 airfoil

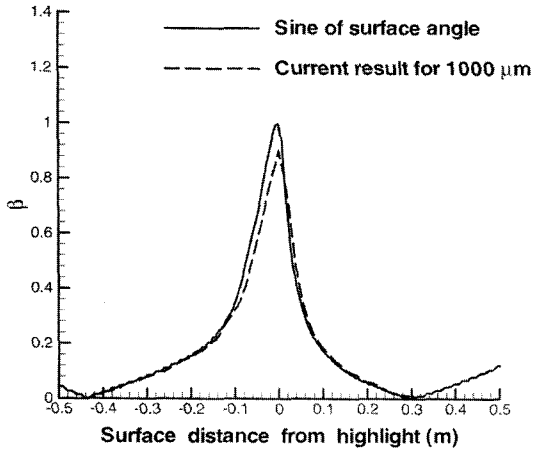

Fig. 6 Comparison of collection efficiency distribution for MVD=1000 μm with theoretical limit

This collection efficiency that resulted from current numerical simulations was compared to that found by Papadakis et al. in his experiments (Papadakis et al., 2003). Prior to the investigation of the characteristics of various particle sizes, the effect of the critical parameters such as integration time-step and number of particles injected from nozzles upstream of the test section portion was evaluated by simulations of several cases, which was able to finalize the appropriate parameters. For the MS-0317 airfoil at zero angle of attack, the collection efficiency distributions over this airfoil surface in simulations with different numbers of droplets for MVD of 79 microns are presented with experimental data in Fig. 7. The figure shows the collection efficiency as a function of the distance along the airfoil surface from the leading edge termed highlight. Airfoil surface distance was negative along the suction side (typically the airfoil upper surface) and positive along the pressure side. Comparison

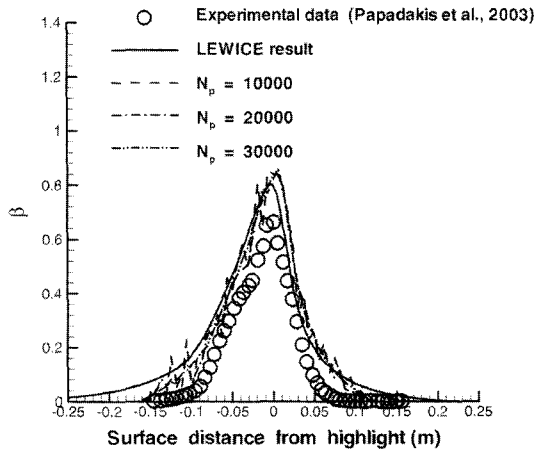

Fig. 7 Comparison of current numerical results for collection efficiency distribution of the different number of particles to the experimental data of Papadakis et al. (2003) and LEWICE results

of the data shows clear and consistent correlation between the collection efficiency determined by the current numerical simulation and the experimental evidence. Note that the plot of the collection efficiency in the fewer particle case (N_p= 10000) produces more "noise" than the reference particle case of N_p=30000. This is a consequence of the statistical nature of the simulation and of the methodology for computing the collection efficiency. The NASA Glenn LEWICE code has been known as a water droplet trajectory and ice accretion code. The results provided by LEWICE and current particle trajectory code developed herein exhibit a similar trend with that observed in the experimental results. The limits of impingement extent of the LEWICE result seem higher than the current numerical result in this case.

In general, increasing the number of particles in the simulation reduced the noise in the results of the collection efficiency. However, for any given number of particles dispersed it is possible to decrease the statistical noise by optimizing the integration time step used in the simulation. Figure 8 shows several plots of the collection efficiency for the same 30000 particle case while varying a non-dimensional time-step parameter

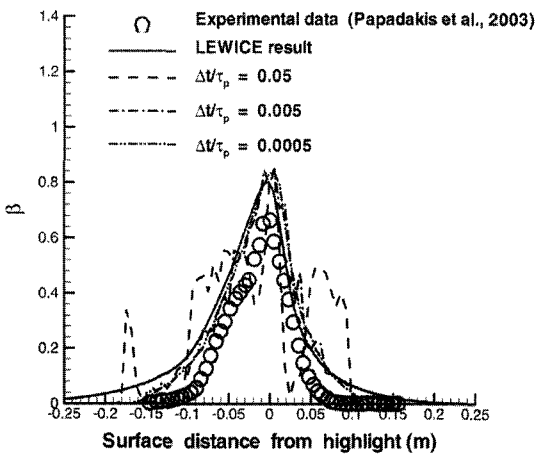

Fig. 8 Comparison of current numerical results for collection efficiency distribution of the different integration time-step to the experimental data of Papadakis et al.(2003) and LEWICE results

obtained by normalizing the integration time-step with τ_p, the particle response time. The results confirm that the maximum time step should be of an order of a hundredth of τ_p or less in order to fully capture all the fluid-particle interactions and minimize the level of noise in the collection efficiency distribution.

The computational impingement data for various particle sizes provided by the particle trajectory code developed herein were compared with experimental data obtained at the Goodrich IWT (Icing Wind Tunnel) and the NASA Glenn IRT. In Fig. 9(a) the collection efficiency of experimental data (Papadakis et al., 2003) obtained during the 2001 impingement tests for an MVD of 21 microns are compared with the results yielded by the LEWICE and current numerical simulations. The numerical results are in good agreement with the experimental results in Fig. 9(a). The large droplet impingement data shown in Figs. 9(b)-9(d) indicate the trends in impingement characteristics with respect to MVD size, that the maximum collection efficiency is located at the upper surface near the leading edge, and the maximum value and total collection efficiency are increased as the MVD size is increased. The extent of the area impinged on by particles also increases with the increment of the MVD size. In general, the LEWICE and current numerical simulations trends are similar as compared with the experimental data in Figs. 9(b)-9(d). However, the computational maximum values of the collection efficiency were considerably higher than the experimental ones, particularly in the region of the highlight, since these computational methods did not consider the affect of large droplets splashing during the impingement process. Another notable observation in predicting the extent of the impingement limit, comparing the experimental data and the computed results provided by the LEWICE and current numerical simulations, is that the computed impingement limit yielded higher than the experimental results on both the upper and lower surfaces, which is partly attributed to droplet splashing. The LEWICE and current numerical simulations did not consider the effect of the droplet splashing.

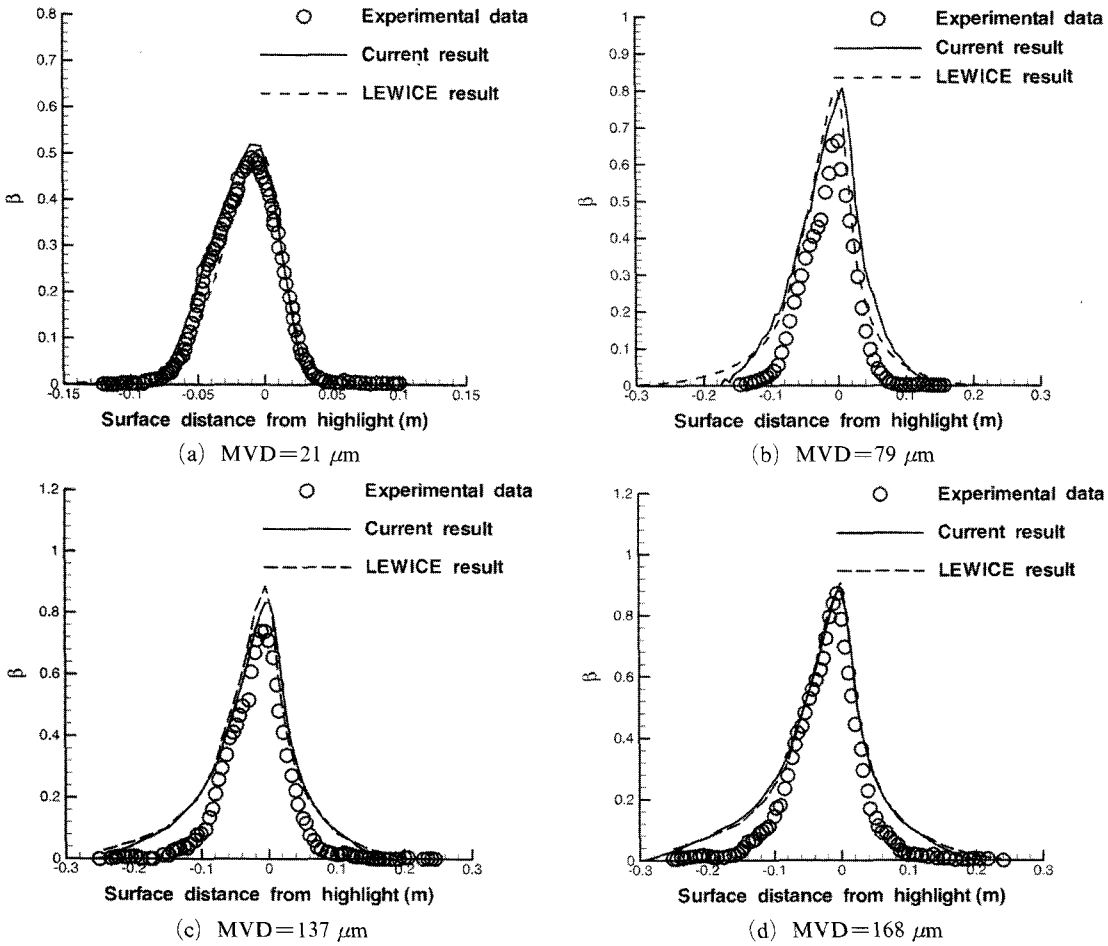

Fig. 9 Comparison of current numerical results for collection efficiency distribution of the different particle sizes to the experimental data of Papadakis et al.(2003) and LEWICE results

The difference between the two computational methodologies, especially in the region of the impingement tails in Fig. 9(b) was partly based on the consideration of turbulent boundary layer development on the airfoil surface, for which the LEWICE adopts a potential flow method to compute the flow field about an airfoil, although the current particle trajectory code uses the simulation results obtained by full Navier-Stokes equation with the SST turbulent model and considers the uncertainty of turbulent flow field by using the CRW method.

4. Conclusions

The aerodynamic effects of leading-edge accretion can raise important safety concerns since the formulation of ice causes severe degradation in aerodynamic performance as compared with the clean airfoil. The NASA Glenn LEWICE code has played a significant role to determine the impingement characteristics and potential ice accretions around the wing. This code adopts the potential flow solver for continuous phases and a Lagrangian transport methodology for droplet phases. Current study provides a methodology to simulate particle trajectory and to scrutinize the impingement characteristics on airfoil surfaces with a viscous flow solver with an Eulerian-Lagrangian transport methodology which is concerned with the turbulent diffusion using Continuous Random Walk method. Computational air-

flow results were produced using the second-order accurate finite volume scheme and the Shear-Stress Transport turbulence model. The airflow was the result of a simulation of the test section portion of the NASA Glenn Icing Research Tunnel installed with an MS-0317 airfoil. The surface pressure coefficients and collection efficiency of the simulated data were compared with the experimental data. The collection efficiency distributions over the airfoil surface in simulations with different numbers of droplets and various integration time-steps for a size were compared with experimental data. The effect of various particle sizes on the collection efficiency was investigated, and the results provided by current numerical simulations exhibited similar trends with that observed in the experimental and LEWICE results. The large droplet impingement data indicated the trends in impingement characteristics with particle size that the maximum value and total collection efficiency were increased as the particle size was increased. The extent of the impingement limit also increased with the increment of the particle size. However, the maximum values of the collection efficiency provided by both computational methods were considerably higher than the experimental ones particularly in the region of the highlight and the impingement tails, since the LEWICE and current simulations did not consider the effect of the big droplet splashing. Further, considering the splashing effect of big droplets, the discrepancy of collection efficiency between experimental and current numerical simulations may be overcome.

Acknowledgments

This work was partly supported by the Brain Korea 21 project.

References

Bragg, M. B. and Khoudadoust, A., 1995, "Study of the Droplet Spray Characteristics of a Subsonic Wind Tunnel," *AIAA Journal of Aircraft*, Vol. 32, pp. 199~204.

Bocksell, T. and Loth, E., 1998, "Stochastic Diffusion Models for Particles in Wakes and Jets," ASME Summer Fluids Engineering Meeting, FEDSM98-5017, Washington, D.C..

DeAngelis, B. C. Loth. E., Lankford, D. and Bartlett, C. S., 1997, "Computations of Turbulent Droplet Dispersion for Wind Tunnel Test," *AIAA Journal of Aircraft*, Vol. 34, No. 2, pp. 2130~2190.

Hancir, P. and Loth, E., 1999, "Computations of Droplet Distribution in the IRT," AIAA 99-0097, 37th AIAA Aerospace Sciences Meeting, Reno, NV, January.

Kim, S. D. and Song, D. J., 2005, "Modified Shear-Stress Transport Turbulence Model for Supersonic Flows," to appear in *AIAA Journal of Aircraft*.

Kuo, K. K., 1986, Principles of Combustion, John Wiley & Sons, New York.

MacInnes, J. M. and Bracco, F. V., 1992, "Stochastic Particle Turbulent Dispersion Modeling and the Tracer-Particle Limit," Physics of Fluids, Vol. 4, No. 2, pp. 2809~2824.

Menter, F. R., 1994, "Two-Equation Eddy-Viscosity Turbulence Models for Engineering Applications," *AIAA Journal*, Vol. 32, No. 6, pp. 1598~1605.

Papadakis, M., Rachman, A., Wong, S., Bidwell, C. and Bencic, T., 2003, "An Experimental Investigation of SLD Impingement on Airfoils and Simulated Ice Shapes," NASA/TM 2003-01-2129.

Snyder, W. H. and Lumley, J. L., 1971, "Some Measurements of Particle Velocity Autocorrelation Functions in a Turbulent Flow," *Journal of Fluid Mechanics*, Vol. 48, pp. 41~71.

Yuu, S., Yasukouchi, N., Hirosawa, Y. and Jotaki, T., 1978, "Particle Turbulent Diffusion in a Dust Laden Round Jet," *AIChE Journal*, Vol. 24, No. 3, pp. 509~519.